An Interactive Technique for Three-Dimensional Image Registration: Validation for PET, SPECT, MRI and CT Brain Studies

Uwe Pietrzyk, Karl Herholz, Gereon Fink, Andreas Jacobs, Rüdiger Mielke, Ina Slansky, Michael Würker and Wolf-Dieter Heiss

Max-Planck-Institut für neurologische Forschung and Klinik für Neurologie der Universität zu Köln, Cologne, Germany

A multipurpose three-dimensional registration technique was validated with PET, SPECT, CT and MRI scans, which had been obtained under normal clinical conditions. In contrast to fully automated procedures, this coregistration method is highly interactive, which has the advantage that it does not impose rigid restrictions by data type and by alterations in normal anatomy or brain function resulting from disease. **Methods:** Basically, a computer program provides a variety of tools to examine the accuracy of coregistration visually and to specify necessary translations and rotations in all three dimensions. Tools and criteria to accept coregistration were applied according to a standardized protocol. Reproducibility was assessed with five independent users on nine pairs of image sets. In two pairs of these image sets, coregistration was repeated three times by each user. **Results:** Depending on the resolution of the images involved, the reproducibility of translation distances ranged from 0.32 to 2.22 mm (s.d.) and of rotation angles from 0.32 to 1.70 degrees. It was always much smaller than the point-spread full-width half maximum of the device with the lower resolution. The accuracy of coregistration was examined using two arbitrarily misplaced image sets. Interindividual and intraindividual variance were similar, which suggested that the influence of subjectivity was not significant. Average displacements after coregistration were 0.43 and 0.29 mm or less for PET and MRI data, respectively, which indicated the absence of a systematic bias. **Conclusion:** The results indicate the high reproducibility and accuracy of this three-dimensional coregistration technique, which is comparable or superior to those of automated techniques and methods based on external artificial landmarks.

Key Words: brain; CT; emission CT; magnetic resonance tomography; three-dimensional; registration

J Nucl Med 1994; 35:2011–2018

In modern medical diagnostics, patients often pass a series of examinations that provide complementary information about a specific part of the human body. For instance, PET or SPECT provide functional information, whereas MRI and x-ray CT mainly demonstrate morphology. For exact anatomic localization of brain function, follow-up and multiple tracer studies and coregistration of the various functional and morphologic images is desirable. However, tomograms usually differ in orientation, scaling and pixel size and cannot be superimposed onto each other without further processing.

There are several approaches described in the literature on the registration of images. Many involve special devices, such as individually prepared head holders, face masks or stereotactic head frames (*1–9*). Usage of such devices, however, may often be impractical and requires detailed coordination of the investigations in advance to ensure that the proper device is used for all imaging modalities. This is often not possible during a clinical diagnostic workup because the decision to have an additional study (e.g., PET) may depend on the results of the previous study (e.g., CT). Therefore, methods that rely on internal landmarks that are visible on brain slices from all methods are clearly more useful in clinical practice (*10–13*). A procedure with different surface models of the head that can be applied to PET, CT and MRI was proposed by Pelizzari et al. (*14,15*). The measure to be minimized is the volume between the individual brain models. Other measures are based on the difference between two data sets or rely on the calculation of the principal axis, regarding the pixels of the brain as a rigid body (*16–18*). Common to all these methods is that they do not rely on some kind of artificial external landmark, and thus can be applied retrospectively. In recent publications (*19–21*), emphasis has been placed on the fact that the procedures proposed therein run fully automatically; in particular, this facilitates the registration of studies that consist of multiple scans. However, all automatic algorithms seem to be restricted to specific organs and image modalities.

In an earlier report (*22*), the authors described a more universally applicable technique for three-dimensional alignment of functional and morphologic tomograms. In contrast to fully automated procedures, this program provides a variety of graphic tools to examine matching accuracy, and the user selects translations and rotations to achieve image registration. The user of the system must be

Received Dec. 10, 1993; revision accepted May 27, 1994.

For correspondence or reprints contact: Prof. Dr. W.-D. Heiss, Max-Planck-Institut für neurologische Forschung, Gleueler Str. 50, D-50931 Köln, FRG.

familiar with the anatomy of the organ investigated and with the principles and limitations of the applied imaging modalities, and thus the final result might bear some subjectivity. In the present study, tools and coregistration criteria were applied according to a standard protocol, and data are reported on the reproducibility and accuracy of this procedure using various combinations of PET, SPECT, MRI and CT images to validate its clinical application.

METHODS AND MATERIALS

Data Processing

The basic principle of the registration technique was described in detail in a previous publication (*22*). Since then, some modifications and extensions were introduced by porting the program to a SUN SPARCstation (SUN Microsystems, Mountain View, CA) operated under UNIX/SUNOS 4.1.2 and OPENWINDOWS 3.0 software. The algorithms for image reorientation and interpolation were written in C; in addition, display and image processing routines of the PV-Wave software package (Visual Numerics, Boulder, CO) were also used for implementation. The time needed to calculate a reoriented cut on a SUN SPARCstation IPX with a 32-megabyte memory is less than 1 sec. Thus, a display update for immediate visual examination of each reorientation step is shown within a few seconds.

Throughout the image registration procedure, the original data are kept unmodified, and each new interpolation for the display of specific cut relates to these original data. For display, images are sampled by three-dimensional linear interpolation into a 128 × 128 or 256 × 256 matrix with a 2- or 1-mm pixel size, respectively. After completion of the matching process, a variety of formats is available to store the registered dataset, again created by trilinear interpolation with sampling from the original data.

The framework of tools provided by the program is illustrated in Figure 1. After loading the two image sets into memory, a first display of three orthogonal slices from each dataset is shown using default parameter settings (Fig. 2A). Then all structures that are relevant to judge the accuracy of coregistration can be displayed subsequently by selecting an appropriate number, orientation (parallel or orthogonal) and level of slices to be displayed simultaneously. To determine the correspondence of anatomic landmarks, a "dual cursor" can be moved in all three dimensions and shown on both image sets. Most powerful is the exchange of contours (Fig. 2B) between image sets to determine matching of the brain surface and major sulci. Contours are not drawn manually but are extracted by conventional edge-detection techniques. The simplest and fastest approach of the several types implemented is thresholding to generate a binary image (i.e., an image that contains ones for pixels above the threshold and zeros elsewhere) with subsequent detection of the change from zero to one. Prior to exchange of the contours of reference and resliced images, the appropriate threshold applied should be verified to ensure they delineate the most characteristic structures in the original image from which they have been derived. Other techniques implemented include the calculation of multiple contours at different thresholds between a predefined range and the algorithm used by Pietrzyk et al. (*22*) developed by Marr and Hildreth (*23*), which in the scientific literature is often referred to as the detection of so-called zero crossings. The latter technique is computationally more extensive but offers more flexibility as it does not require the definition of a lower threshold. New rotation angles and translations can be specified by keyboard or by an arrow box (Fig. 3) or are calculated within a selected plane by identification of two anatomic landmarks on each of the two image sets. After each operation, the display is updated, and the process is iterated until coregistration is achieved (Fig. 2C). Then an integrated display obtained by image fusion, based on a two-dimensional color-lookup table (*24*), may be used to show the final result for clinical interpretation (Fig. 2D), and the resliced data set may be saved on disk.

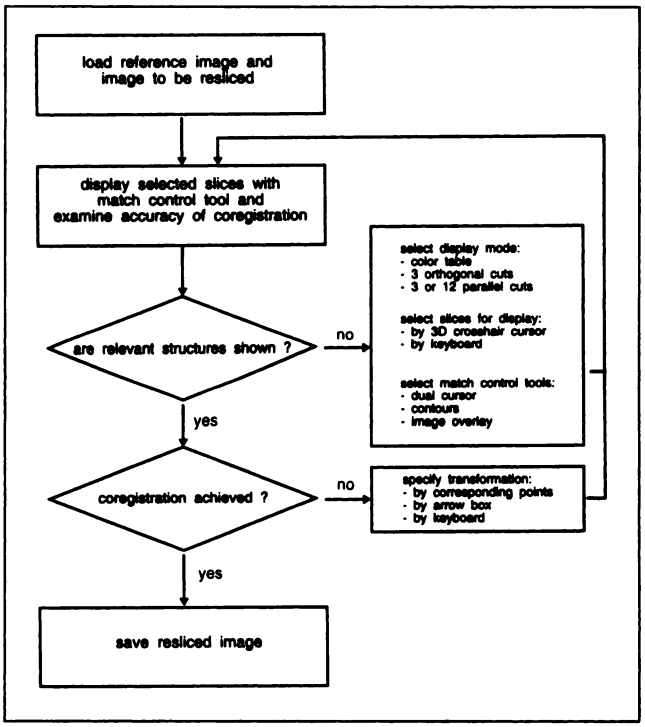

FIGURE 1. Basic flow chart. Although the user can freely select from the list of options available. The displayed flow control, as shown in this figure, turned out to be the most useful.

Although not strictly required by the design of the registration technique presented here, a specific order of usage of these tools was the most effective and was followed in this validation study. First, three orthogonal sections were displayed, i.e., transaxial (approximately at the level of the basal ganglia), midsagittal and midcoronal (Fig. 2A). Second, anatomic landmarks points were marked on each of the two sets of images to achieve gross coregistration, i.e., the frontal and occipital pole on the transaxial cut, the two points of largest curvature at the edge from lateral to inferior aspect of both temporal lobes on the coronal cut and the frontal pole and indentation between the occipital pole and cerebellum on the sagittal cut. Third, contours of brain surface were displayed (adjust thresholding levels, if necessary), and their positions were compared by overlay on each other (Fig. 2B). New rotation or translation was specified, if necessary. This was performed repeatedly on orthogonal cuts in at least two positions, including coronal cuts through the frontal and occipital lobe and parasagittal cuts through the basal ganglia on both sides of the brain, until a match that could not be improved further was achieved. In addition, the correspondence of specific landmarks (e.g., scalp and other extracerebral structures, ventricles, ambient cistern, interhemispheric cleft, sylvian fissure, basal ganglia and

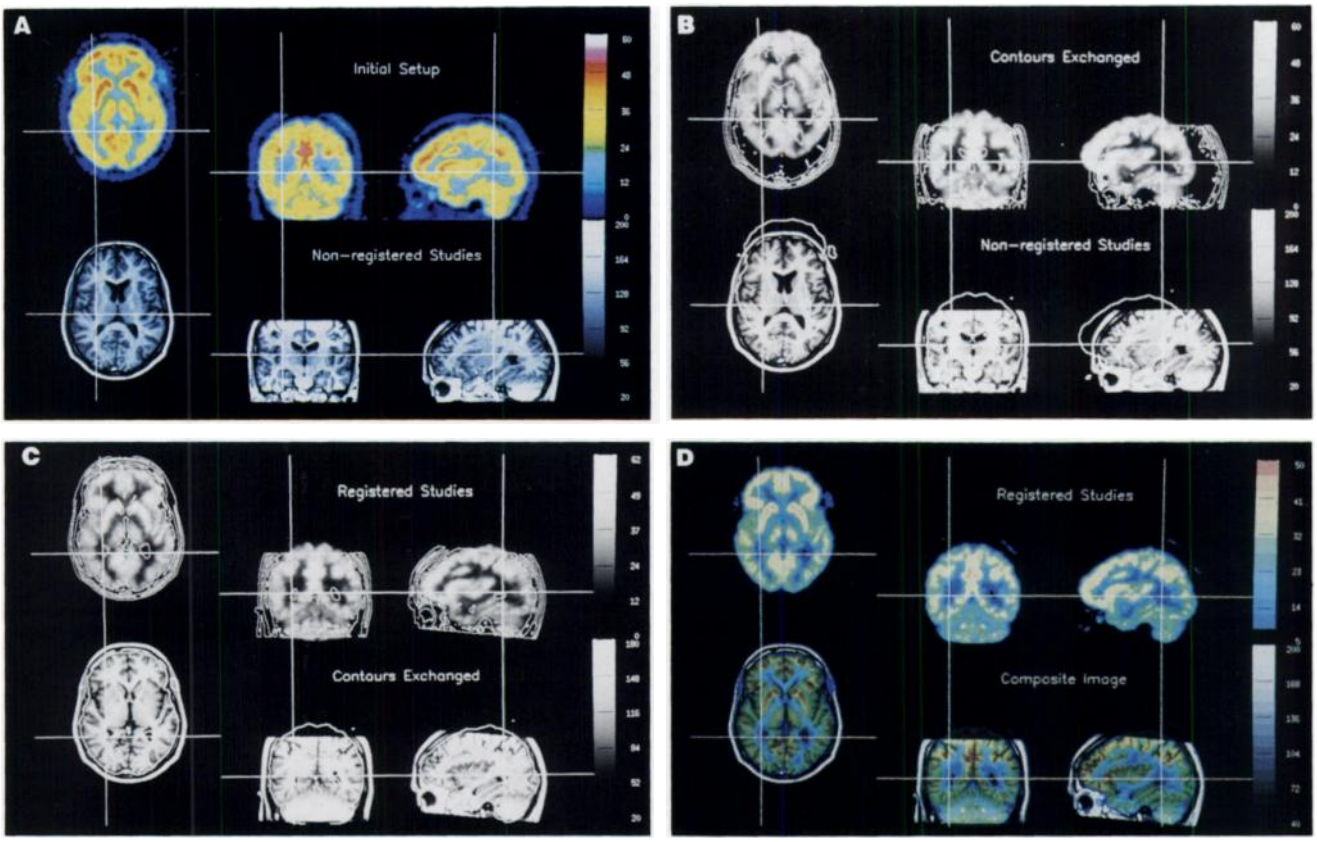

FIGURE 2. (A) Initial setup. Top row shows three orthogonal cuts of a PET study, which serve as reference data. Bottom row shows data from a second study (in this case, MRI). Second study is not yet aligned with respect to the reference data. (B) Tools to examine the accuracy of coregistration. Same studies as in part (A) are displayed but with the contours of each dataset exchanged. Contours from the images in the upper row now are superimposed on the images in the lower row and vice versa. (C) Registered studies. Studies are the same as in part (A) and (B). Here contours are exchanged as in part (B), but appropriate action, as described in the text, has coregistered the MRI study with respect to a PET study. (D) Integrated display. Registered PET and MRI studies may be displayed as composite images obtained by image fusion, based on a two-dimensional color-lookup table (*24*). Basically, the color is driven by the PET pixel content, whereas the intensity is selected according to the gray level of the MRI pixel.

thalamus and the border between the corpus callosum and the cingulate gyrus) was checked with the dual cursor to clarify residual ambiguities, if necessary. Fourth, 12 cuts, transaxial coronal or sagittal, were displayed for final examination, and the resliced dataset was stored.

Finding the best visual match between the reference and resliced data corresponds mathematically to the determination of a set of the three translations and three rotations which are required to move an object in three-dimensional space. The more similar the resulting tomograms of independent alignment sessions are, the more similar are the two sets of parameters. Storing these parameters on disk thus allows a detailed analysis of registration accuracy and reproducibility, when performed by several users, as in the present comparative study.

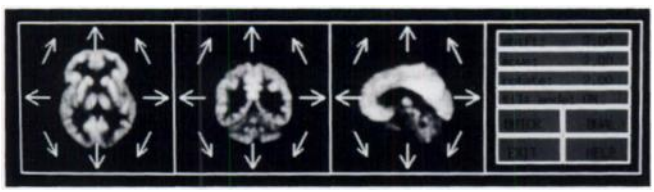

FIGURE 3. Selection panel that shows the typical display of three orthogonal cuts. Arrows are placed accordingly to depict the action the user can initiate by pointing with a location device (mouse) to a particular arrow.

Data

PET data were acquired after intravenous injection of ^{18}F-2-deoxy-2-fluoro-D-glucose (FDG), ^{15}O-labeled water or ^{18}F-6-fluoro-L-dopa (F-Dopa). Two different scanners were used. A four-ring scanner (Scanditronix PC 384, Uppsala, Sweden) that produced seven slices with transaxial resolution of 7.8 mm full-width half maximum (FWHM) and approximately 11-mm slice thickness (*25*). With this scanner, two sets of interleaved slices were acquired, yielding a total of 14 slices with a 6.85-mm center-to-center distance and an axial field of view of 10 cm. The other scanner (ECAT EXACT, Siemens-CTI, Knoxville, TN) provided 47 overlapping slices with a transaxial resolution of 6.0-mm FWHM, approximately 5-mm slice thickness and a 3.375-mm center-to-center distance (*26*). The axial field of view extended over 16.2 cm, covering the entire brain.

SPECT data were acquired with a single-head rotating gamma camera (Orbiter 37, Siemens Medical Systems, Erlangen, Germany) equipped with a focusing collimator (Neurofocal) after intravenous injection of ^{99m}Tc-hexamethylpropyleneamineoxime (HMPAO).

MRI scans were acquired on a 1.0-T superconducting instru-

TABLE 1
Summary of Essential Parameters for Each Study

Study	Modality	Tracer	Dose (mCi)	Type	FWHM (mm)	Slices	Pixel size (mm)	Slice distance (mm)	Matrix	Diagnosis
A	PET	FDG	10	Reference	6.0/5.0	47	2.1	3.375	128	Normal
	PET	DOPA	10	Resliced	6.0/5.0	47	2.1	3.375	128	Normal
B	PET	H_2O	40	Reference	6.0/5.0	47	2.1	3.375	128	Infarct
	PET	H_2O	40	Resliced	6.0/5.0	47	2.1	3.375	128	Follow-up
C	PET	FDG	10	Reference	6.0/5.0	47	2.1	3.375	128	Dementia
	PET	FDG	10	Resliced	6.0/5.0	47	2.1	3.375	128	Resting vs. activation
D	PET	FDG	10	Reference	6.0/5.0	47	2.1	3.375	128	Dementia
	SPECT	HMPAO	20	Resliced	11.0/11.0	70	3.2	3.2	128	Dementia
E	PET	FDG	5	Reference	7.0/11.4	14	2.55	6.85	128	Tumor
	CT			Resliced	*	40	1.15	2.0	256	Tumor
F	PET	FDG	5	Reference	7.0/11.4	14	2.55	6.85	128	Dementia
	MRI (FLASH)			Resliced	*	63	1.0653	2.0	256	Dementia
G	PET	FDG	10	Reference	6.0/5.0	47	2.1	3.375	128	Dementia
	MRI (FLASH)			Resliced	*	63	1.0653	2.0	256	Dementia
H	PET	FDG	10	Reference	6.0/5.0	47	2.1	3.375	128	Normal
	PET	FDG	10	Resliced	6.0/5.0	47	2.1	3.375	128	Normal
I	MRI (FLASH)			Reference	*	63	1.0653	2.0	256	Dementia
	MRI (FLASH)			Resliced	*	63	1.0653	2.0	256	Dementia

*Not relevant.

ment, using a standard head coil (Magnetom, Siemens Medical Systems) and a T1-weighted fast low-angle shot sequence with an echo time of 15 msec, repetition time of 40 msec and flip angle of 40°. Sixty-four contiguous transaxial slices with a 2-mm slice thickness were recorded in 256 × 256 matrices with a 1-mm pixel size.

X-ray CT scans were acquired on a Somatom DR 2 (Siemens Medical Systems) also in 256 × 256 matrices of 1.15-mm pixel size, 4-mm slice thickness with 2-mm table increments. A total of 40 slices were recorded, resulting in a axial field of view of 8 cm.

All reconstructed images were stored in digital format. CT and MRI data were transferred for evaluation to the PET laboratory by ethernet, streamer tape or conventional magnetic tape.

Nine pairs of patient datasets were selected, representing typical clinical applications (Table 1). In seven of these study pairs (A to G), two sets of images of the same subject, but recorded separately, were coregistered. This was done independently by five experienced users of the program, and the reproducibility of the results was analyzed. In two of these study pairs (C and G), coregistration was repeated by each user three times on different days. Thus, intraindividual variability of the results was also determined and compared with interindividual variability. In the remaining two study pairs (H and I), the image to be coregistered was derived from the reference image by arbitrary reorientation. In these two studies, coregistration was equivalent to restoring the original image, and thus the accuracy of the coregistration process was determined.

The transformation parameters from all registration sessions of all users in the present study were analyzed by calculating mean and s.d. (study pairs H and I) or s.d. (study pairs A to G) of translation distances and rotation angles in all three dimensions. For study pairs A to G, there are, by definition, no true values for the transformation parameters available; hence, the accuracy was assessed by comparing the final registration parameter sets of all users by calculating the respective s.d. The smaller the s.d., the more identical the final resliced images.

For study pairs H and I, the true values were known, and the results from the registrations could be directly compared with them by calculating the mean differences of the transformation parameters and their respective true values. In addition, the s.d. of the mean differences were calculated. The intersection of the three rotation axes was located in the center of the reference data set. In addition, linear misplacement was also calculated at five selected points in the central transaxial plane, corresponding approximately to the anterior, posterior, right lateral and left lateral pole of the brain and to its center.

RESULTS

Reproducibility was best for coregistration of the FDG-PET activation study with the corresponding resting study (C). Angular s.d.s were 0.54 degrees or less, and translation s.d.s were 0.56 mm or less (Table 2). A similar result was obtained for coregistration of an arbitrarily misplaced FDG-PET image set with the original (H), with very low values for average misalignment (rotation angles 0.43 degrees or less and translation distance of 0.43 mm or less). Similar or even slightly better results were obtained for coregistration of a misplaced MRI image dataset with its original (I). In all these studies, means and s.d.s of the linear misalignments in the five selected brain areas were generally less than 1 mm (Table 3).

Coregistration of different imaging modalities or of PET blood flow studies, which are significantly noisier than FDG studies, resulted in approximately two to four times larger s.d. Nevertheless, the s.d. of rotation angles and translation distances was usually less than 2 degrees or 2

TABLE 2
Results from Validation Study Considering the Three Angles of Rotation and Three Translations

	Studies	Alpha (AP‡) (degree)	Alpha (RL§) (degree)	Alpha (axial) (degree)	d (AP) (mm)	d (RL) (mm)	d (axial) (mm)
A	PET vs. PET* (FDG vs. DOPA)	0.99	1.08	0.32	1.65	1.45	1.18
B	PET vs. PET* (H_2O vs. H_2O)	1.27	1.45	1.02	1.79	1.48	0.62
C	PET vs. PET* (FDG vs. FDG)	0.43	0.54	0.54	0.32	0.56	0.55
D	PET vs. SPECT* (FDG vs. HMPAO)	1.22	1.70	0.63	1.81	1.83	0.90
E	PET vs. CT* (FDG)	1.38	1.30	0.35	0.99	1.13	2.22
F	PET vs. MRI* (FDG vs. FLASH-3D)	1.32	1.45	0.68	1.55	1.64	1.03
G	PET vs. MRI* (FDG vs. FLASH-3D)	1.68	0.51	0.57	0.98	0.83	1.71
H	PET vs. PET'† (FDG vs. FDG)	0.19 (0.25)	0.43 (0.42)	0.17 (0.23)	−0.25 (0.22)	−0.43 (0.53)	−0.05 (0.18)
I	MRI vs. MRI'† (FLASH-3D vs. FLASH-3D)	0.01 (0.13)	0.13 (0.34)	−0.08 (0.45)	0.08 (0.36)	0.29 (0.34)	0.12 (0.24)

*S.d. of the three angles and translations.
†Difference of average rotation and translation and true standard. The s.d. is in parentheses.
‡Around the anterior-posterior axis.
§Around the right-left lateral axis.

mm, respectively. For instance, in the coregistration of FDG-PET with F-Dopa PET (A), brain contours were less clearly evident on the F-Dopa image than of the FDG image because F-Dopa is preferentially taken up by the basal ganglia. With appropriate thresholds, however, contours were still sufficiently well identified to achieve reproducible coregistration (Fig. 4). In the coregistration of FDG-PET with HMPAO-SPECT (D), the relatively poor resolution of the SPECT images limited the accuracy of coregistration, but still both techniques showed high tracer uptake in cortical structures, and thus, a reasonable delineation of the outer brain contour is possible. A difficulty in the coregistration of FDG-PET and CT (E) was caused by the limited axial view of only 8 cm in this particular CT study. Thus, only parts of the brain contour were available to check image registration, resulting in the largest axial translation variance (s.d. = 2.22 mm) recorded in this validation series. There were two study pairs of FDG-PET and MRI (F and G) involving PET scanners with different resolution. This difference, however, had only a minor impact on the results, and s.d. were not uniformly smaller in the study with the higher resolution.

Interindividual variance in repeated coregistration (C and G) was slightly larger than intraindividual variation for all parameters (Table 4), except for the anterior-posterior inclination, the differences were not significant (F test), which indicated that the subjective influence on the results was small.

The time needed to complete coregistration of one study pair varied considerably, ranging between 10 and 30 min (median 25 min). Gross coregistration was usually achieved within 5 to 15 min, and the remainder of the time was spent on making minor adjustments of 2 mm or less.

DISCUSSION

In contrast to fully automated procedures (*19–21*), this coregistration method is highly interactive, which has the advantage that it does not impose major restrictions by image type and by alterations of normal anatomy or brain function resulting from disease. There is also no requirement for a clear identification of the interhemispheric plane in regard to its specific shape as in the method described by Kapouleas et al. (*13*). This is especially important in studies with F-Dopa-PET, as shown in Figure 4. An unambiguous identification of the interhemispheric plane would be difficult, if not impossible, and hence unreliable. However, with the appropriate selection of contours by thresholding and filtering, there are still sufficient details visible, such as the curvature of the overlaid contours, which nicely delineate characteristic brain structures, to which the human visual system can easily attach and, thus, detect even smaller misalignments. This method simply can omit the unique identification of specific landmarks or reference points but can easily rely on the ample amount of structures and curvatures of contours present in medical images. The display of three orthogonal views eases the detection of even small misplacements with respect to any orientation. Indeed, the outline of a brain may be incomplete in one modality because of functional deactivations

TABLE 3
Results from Validation Study Considering the Residual Uncertainty in Three Dimensions at Selected Positions

	Studies	Coordinate	d (ant) (mm)	d (post) (mm)	d (right) (mm)	d (left) (mm)	d (center) (mm)
A	PET vs. PET*	x	0.78	0.86	1.15	0.54	0.81
	(FDG vs. DOPA)	y	0.73	0.94	0.73	0.77	0.75
		z	0.91	2.15	1.40	1.97	1.18
B	PET vs. PET*	x	0.86	0.89	1.62	1.36	0.85
	(H_2O vs. H_2O)	y	1.26	1.21	0.48	0.19	0.20
		z	1.26	1.89	1.17	2.41	0.62
C	PET vs. PET*	x	0.56	0.50	0.77	0.88	0.53
	(FDG vs. FDG)	y	0.40	0.91	0.31	0.28	0.29
		z	0.48	0.94	0.62	0.97	0.55
D	PET vs. SPECT*	x	1.04	1.11	0.82	1.74	0.85
	(FDG vs. HMPAO)	y	1.14	1.26	0.36	0.51	0.43
		z	2.20	2.28	3.16	3.19	0.90
E	PET vs. CT*	x	0.86	0.76	0.98	0.87	0.80
	(FDG)	y	1.14	0.85	0.86	0.93	0.90
		z	2.44	3.17	1.77	3.53	2.22
F	PET vs. MRI*	x	1.16	1.57	0.99	1.94	1.32
	(FDG vs. FLASH-3D)	y	1.48	1.66	1.30	1.39	1.35
		z	2.30	1.19	2.62	1.07	1.03
G	PET vs. MRI*	x	0.92	0.55	1.16	0.63	0.70
	(FDG vs. FLASH-3D)	y	0.29	1.13	0.56	0.51	0.53
		z	1.68	3.08	2.00	1.64	1.71
H	PET vs. PET'†	x	0.04 (0.29)	−0.03 (0.29)	−0.26 (0.31)	0.27 (0.59)	0.01 (0.28)
		y	0.15 (0.51)	−0.38 (0.36)	−0.06 (0.24)	−0.17 (0.25)	−0.11 (0.24)
		z	−0.28 (0.44)	0.18 (0.39)	−0.75 (0.79)	0.65 (0.57)	−0.05 (0.18)
		r	0.32 (0.45)	0.43 (0.37)	0.80 (0.75)	0.73 (0.56)	0.13 (0.23)
I	MRI vs. MRI'†	x	0.07 (0.25)	0.07 (0.27)	0.17 (0.68)	−0.02 (0.48)	0.07 (0.26)
		y	−0.25 (0.67)	−0.06 (0.56)	−0.14 (0.34)	−0.17 (0.30)	−0.16 (0.32)
		z	0.12 (0.17)	0.11 (0.38)	0.26 (0.53)	−0.03 (0.49)	0.11 (0.24)
		r	0.29 (0.59)	0.14 (0.39)	0.34 (0.54)	0.17 (0.31)	0.21 (0.29)

*S.d. of three-dimensional coordinates at selected positions within the image matrix.
†Difference of averaged 3D coordinates and true standard at selected positions, distance (r) in 3D space between average and true. The s.d. is in parentheses.

caused by a tumor, as can be seen in Figure 5. The FDG-PET study served as the reference, and methionine-PET and MRI studies were resliced to match the reference FDG study. Again, there are enough features, despite the different outline and tracer uptake in the methionine study, so that this method can provide sufficient clues on which the user can rely by visual inspection and control of the registration process. The price to pay for this broad applicability is some degree of subjectivity in the evaluation of the accuracy of coregistration. However, the similarity of inter- and intraindividual variance suggests that the influence of subjectivity on this procedure is not significant. The authors are not aware of any automated procedure that currently could replace the expertise of a trained human user in recognizing the possible variations of the standard situation caused by technical peculiarities or disease, which might upset pattern recognition programs. In addi-

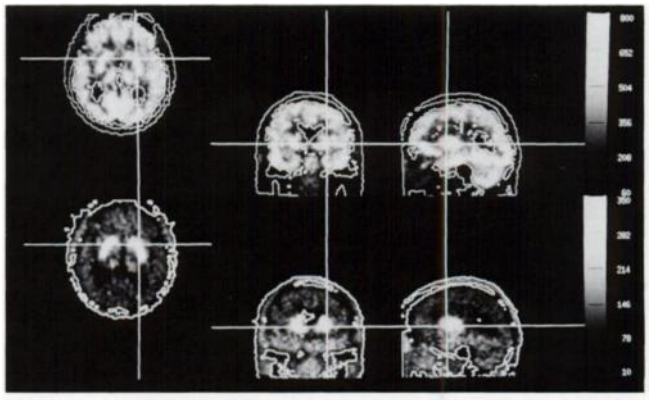

FIGURE 4. Coregistration of FDG-PET with F-Dopa-PET. Although F-Dopa images show preferential uptake in the basal ganglia, appropriate thresholds yield contours sufficiently well identified to achieve reliable coregistration. This is verified by superposition of the exchanged contours.

TABLE 4
Standard Deviations of Intraindividual Versus Interindividual Variation of Registration

	Studies	Alpha (AP) (degree)	Alpha (RL) (degree)	Alpha (axial) (degree)	d (AP) (mm)	d (RL) (mm)	d (axial) (mm)
C	PET vs. PET* (FDG vs. FDG)	0.29 0.54‡	0.46 0.68	0.32 0.43	0.45 0.60	0.63 0.76	0.55 0.56
G	PET vs. MRI* (FDG vs. FLASH-3D)	1.38 1.67	0.99 1.10	0.43 0.45	1.52 1.84	1.16 1.36	0.89 1.46

		Coordinate	d (ant) (mm)	d (post) (mm)	d (right) (mm)	d (left) (mm)	d (center) (mm)
C	PET vs. PET†	x	0.33 0.40	0.32 0.35	0.56 0.65	0.43 0.61	0.33 0.37
	(FDG vs. FDG)	y	0.69 0.61	0.62 0.74	0.54 0.46	0.53 0.44	0.54 0.45
		z	0.66 0.77	0.63 0.93	0.76 0.86	0.78 1.07	0.55 0.56
G	PET vs. MRI†	x	0.68 0.80	0.85 1.04	0.79 0.96	0.95 1.04	0.74 0.87
	(FDG vs. FLASH-3D)	y	0.55 0.65	0.88 0.98	0.59 0.69	0.55 0.65	0.57 0.67
		z	1.35 1.99	2.03 2.59	1.44 1.65	1.39 2.12	0.89 1.46

*s.d. of the three angles and translations (intra- vs. interindividual).
†s.d. at selected locations (intra- vs. interindividual).
‡$p < 0.05$ in F test on variances.

tion, it was pointed out by the authors of an automated registration procedure (*20*) that the final result should always undergo a visual inspection to avoid possible failures of the applied algorithms. Image resolution is certainly a major factor that influences the results, as indicated by the relatively high variability of PET/SPECT coregistration. However, the variability of coregistration was always considerably smaller than the point-spread FWHM of the functional images involved. Because reasonable quantitation of functional images should always be based on regions larger than the corresponding point-spread FWHM to achieve recovery coefficients of better than 50% (*27*), the lower variability of coregistration should not have a major impact. The presence of systematic displacements, which could cause significant bias even if small, was ruled out by the accurate realignment of arbitrarily misplaced datasets in study pairs H and I.

These values compare well with published results obtained with automated procedures (*15,19,20*) in which values concerning the registration of PET versus PET within approximately 1.7 mm (*19*) and of PET versus MRI within 2.48 mm (*15*), 2.3 mm (*20*) and maximal 3 mm (*21*), respectively, were quoted. For procedures that use external markers (head frames or face masks), the values range from 1.0 mm (*8*) for the registration of PET versus MRI based on phantom studies to 2.5 mm (*9*) for PET, CT and MRI registration based on patient data.

Only a basic knowledge of neuroanatomy is required from the user of this interactive procedure, i.e., the ability

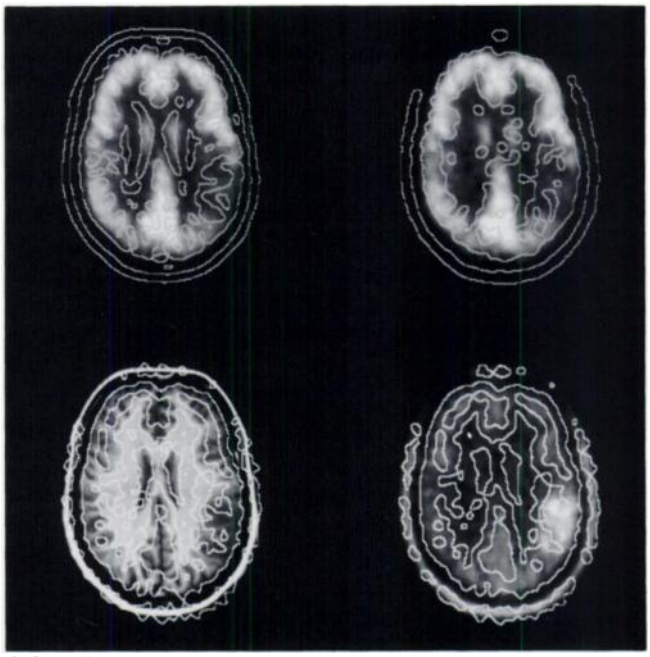

FIGURE 5. Coregistration of methionine-PET and MRI with a FDG-PET study, which served as reference. Despite the relatively different tracer uptake in the methionine-PET study, sufficient outlines in either study are presented to the user to visually inspect and control the registration process. Contours are exchanged between the FDG and MRI studies and FDG and methionine respectively. Top left: FDG-PET with contours from MRI. Top right: FDG-PET with contours from methionine-PET. Bottom left and right: contours from FDG-PET superimposed onto MRI and methionine-PET, respectively.

to identify major lobes, the ventricular system and brainstem. However, more knowledge about imaging characteristics is essential. The user should be familiar with rules governing the intensity or signal of cerebral and extracerebral structures in different imaging modalities.

In conclusion, the results indicate that the reproducibility and accuracy of this universal three-dimensional coregistration technique is comparable or superior to those of published automated techniques or those based on head holders or face masks, but the technique does not impose most of their limitations. The technique is therefore validated for use in normal persons and in patients with brain disease.

REFERENCES

1. Bergström M, Boethius J, Eriksson L, et al. Head fixation device for reproducible positron alignment in transmission CT and positron emission tomography. *J Comput Assist Tomogr* 1981;5:136–141.
2. Mazziotta JC, Phelps ME, Meadors AK, et al. Anatomical localization schemes for use in positron computed tomography using a specially designed headholder. *J Comput Assist Tomogr* 1982;6:848–853.
3. Kearfott KJ, Rottenberg DA, Knowless RJR. A new headholder for PET, CT, and NMR imaging. *J Comput Assist Tomogr* 1984;8:1217–1220.
4. Schad LR, Boesecke R, Schlegel W, et al. Three dimensional image correlation of CT, MR, and PET studies in radiotherapy treatment planning of brain tumors. *J Comput Assist Tomogr* 1987;11:948–954.
5. Evans AC, Beil C, Marrett S, Thompson CJ, Hakim A. Anatomical-functional correlation using an adjustable MRI-based region of interest atlas with positron emission tomography. *J Cereb Blood Flow Metab* 1988;8:513–530.
6. Miura S, Kanno I, Iida H, et al. Anatomical adjustment in brain positron emission tomography using CT images. *J Comput Assist Tomogr* 1988;12: 363–367.
7. Wilson MW, Mountz JM. A reference system for neuroanatomical localization on functional reconstructed cerebral images. *J Comput Assist Tomogr* 1989;13:174–178.
8. Meltzer CC, Bryan RN, Holcomb HH, et al. Anatomical localization for PET using MR images. *J Comput Assist Tomogr* 1990;14:418–426.
9. Bettinardi V, Scardaoni R, Gilardi MC, et al. Head holder for PET, CT, and MR studies. *J Comput Assist Tomogr* 1991;15:886–892.
10. Martin WRW, Grochowski E, Palmer M, Pate BD. Correlation of structural and functional images in the same patient. *J Nucl Med* 1987;28:634.
11. Maguire GQ, Noz ME, Lee EM, Schimpf JH. Correlation methods for tomographic images using two- and three-dimensional techniques. In: Bacharach SL, ed., *Information processing in medical imaging*. Dordrecht: Martinus Nijhoff; 1985:266–279.
12. Evans AC, Marrett S, Collins L, Peters TM. Anatomical-functional correlative analysis of the human brain using three-dimensional imaging systems. *Proc SPIE* 1989;1092:264–274.
13. Kapouleas I, Alavi A, Alves WM, Gur RE, Weiss DW. Registration of three-dimensional MR and PET images of the human brain without markers. *Radiology* 1991;181:731–739.
14. Pelizzari CA, Chen GTY, Halpern H, Chen CT, Cooper MD. Three-dimensional correlation of PET, CT and MRI images. *J Nucl Med* 1987;28:682.
15. Pelizzari CA, Chen GTY, Spelbring DR, Weichselbaum RR, Chen CT. Accurate three-dimensional registration of CT, PET, and/or MR images of the brain. *J Comput Assist Tomogr* 1989;13:20–26.
16. Alpert NM, Bradshaw JF, Kennedy D, Correia JA. The principal axes transformation—a method for image registration. *J Nucl Med* 1990;31:1717–1722.
17. Phillips RL, London ED, Links JM, Cascella NC. Program for PET image alignment: effects on calculated differences in cerebral metabolic rates for glucose. *J Nucl Med* 1990;31:2052–2057.
18. Mintun MA, Lee KS. Mathematical realignment of paired PET images to enable pixel-by-pixel subtraction. *J Nucl Med* 1990;31:816.
19. Woods RP, Cherry SR, Mazziotta JC. Rapid automated algorithm for aligning and reslicing PET images. *J Comput Assist Tomogr* 1992;16:620–633.
20. Woods RP, Mazziotta JC, Cherry SR. MRI-PET registration with automated algorithm. *J Comput Assist Tomogr* 1993;17:536–546.
21. Steinmetz H, Huang Y, Seitz RJ, et al. Individual integration of positron emission tomography and high-resolution magnetic resonance imaging. *J Cereb Blood Flow Metab* 1992;12:919–926.
22. Pietrzyk U, Herholz K, Heiss W-D. Three-dimensional alignment of functional and morphological tomograms. *J Comput Assist Tomogr* 1990;14:51–59.
23. Marr D, Hildreth E. Theory of edge detection. *Proc R Soc Lond B* 1980; 207:187–217.
24. Pietrzyk U. A rapid three-dimensional visualization technique to evaluate function in relation with anatomy of the human cortex. In: Klaisner L, ed. 1993 IEEE conference record. Nuclear science symposium and medical imaging conference. NY: IEEE; 1994:1810–1812.
25. Eriksson L, Bohm C, Kesselberg M, et al. A four ring positron camera system for emission tomography of the brain. *IEEE Trans Nucl Sci* 1982; 29:539–543.
26. Wienhard K, Eriksson L, Grootonk S, et al. Performance evaluation of the positron scanner ECAT EXACT. *J Comput Assist Tomogr* 1992;16:804–813.
27. Hoffman EJ, Huang S-C, Phelps ME. Quantitation in positron emission computed tomography: 1. Effect of object size. *J Comput Assist Tomogr* 1979;3:299–308.